The Flow Instability Over the Infinite Rotating Disk

Yun-Yong Lee, Young-Kyu Hwang*, Kwang-Won Lee
School of Mechanical Engineering, Sungkyunkwan Univeristy, 300 Chunchun-dong, Jangan-gu, Suwon 440-746, Korea

The hydrodynamic instability of the three-dimensional boundary layer on a rotating disk introduces a periodic modulation of the mean flow in the form of stationary cross flow vortices. The instability labeled Type II by Faller occurs first at lower Reynolds number than that of well known Type I instability. Detailed numerical values of the amplification rates, neutral curves and other characteristics of the two instabilities have been calculated over a wide range of parameters. Presented are the neutral stability results concerning the two instability modes by solving the appropriate linear stability equations reformulated not only by considering whole convective terms but also by correcting some errors in the previous stability equations. The present stability results agree with the previously known ones within reasonable limit. Consequently, the flow is found to be always stable for a disturbance whose dimensionless wave number is greater than 0.75. Some spatial amplification contours have been computed for the stationary disturbance wave, whose azimuth angle $\varepsilon=11.29°$ to 15° and for the moving disturbance wave, whose azimuth angle $\varepsilon=12.5°$ to 15°. Also, some temporal amplification contours have been computed for the stationary disturbance wave, whose azimuth angle $\varepsilon=11.29°$ to 15° and for the moving disturbance wave, whose azimuth angle $\varepsilon=12°$ to 15°. The flow instability was observed by using a white titanium tetrachloride gas over rotating disk system. When the numerical results are compared to the present experimental data, the numerical results agree quantitatively, indicating the existence of the selective frequency mechanism.

Key Words : Kármán boundary-layer flow, Flow Instability, Rotating disk, Spatial Amplification, Temporal Amplification

Nomenclature

A : Constant physical wave number
A_S : Spatial amplification
A_T : Temporal amplification
B : Constant physical frequency
C : cos ε
Co : Coriolis parameter, $Co=2-Ro-Ro^2=2$
Cp : Wave velocity, β_R/α_R
D : A characteristic boundary-layer depth, $D=(\nu/\omega_D)^{1/2}$
D_1 : Boundary-layer thickness, $(Dr)^{1/2}$
J : Scaling factor $[O(1)]$
r : Radius of a disk, $r=\bar{r}/D$
Re : Reynolds number, $Re=\Delta\omega\bar{r}D/\nu$
Ro : Rossby number, $Ro=\Delta\omega/\omega_D$ (for Kármán Boundary-Layer, $Ro=-1$)
S : sin ε
z : Axial coordinates, $z=\bar{z}/D$

Greek symbols

α : Complex wave number, $\alpha=\bar{\alpha}_D$
β : Complex wave frequency, $\beta=\bar{\beta}/\omega_D$
δ : An angle of the new oriented coordinate system, $\delta=\varepsilon+\pi/2$
ε : The azimuth angle of disturbance wave
ξ : Radial components of perturbation vorticity eq.
η : Tangential components of perturbation vorticity

* Corresponding Author,
E-mail : ykhwang@yurim.skku.ac.kr
TEL : +82-31-290-7437; **FAX** : +82-31-290-5849
School of Mechanical Engineering, Sungkyunkwan Univeristy, 300 Chunchun-dong, Jangan-gu, Suwon 440-746, Korea. (Manuscript **Received** March 11, 2003; **Revised** June 25, 2003)

η_∞ : Outer of the boundary-layer
ν : Kinematic viscosity (cm^2/sec)
$\Delta\omega$: A relative angular speed of fluid, $\Delta\omega = -\omega_D$
ω_F : Angular velocity of fluid
ω_D : Angular velocity of disk

Subscripts

c : Critical
D : Disk
F : Fluid
I : Imaginary value
R : Real value
r : With respect to radius, $\partial/\partial r$
t : With respect to time t, $\partial/\partial t$
y : With respect to y, $\partial/\partial y$
z : With respect to z, $\partial/\partial z$
θ : With respect to θ, $\partial/\partial\theta$
∞ : Outer region of the boundary layer
1 : Type I instability
2 : Type II instability

Superscripts

$\bar{}$: Dimensional

1. Introduction

The hydrodynamic stability over the rotating system has been investigated by many scientists in order to understand the fundamental mechanism of 3-dimensional boundary-layer transition process. Those studies have been performed by Wilkinson and Malik (1985), Faller (1991), Kohama and Suda (1993), and, Lingwood (1997). Various types of flows belong to this category. As an example, the stability and transition of rotating flows have been related to aerospace, meteorology, marine applications and similar phenomena over swept-back airfoils such as an impeller and transition process over the rotating wafer surface.

The rotation of flow system dramatically affects the stability characteristics of flows at various physical situations. After the famous exact solution for the Kármán boundary-layer flow were obtained by Sparrow and Gregg (1960), the progress made in stability theory and experiment for rotating flows has been explosive in the past decades. Rogers and Lance (1960) generalized ordinary differential equations for the flow near a rotating disk, assuming that the fluid moves with an angular velocity at infinity. The stability analysis of Lilly (1966) and Faller and Kaylor (1966) for the Ekman layer flow revealed that the inclusion of Coriolis term in the stability analysis for stationary disturbance wave yields the significant increment of the critical Reynolds number, $Re_{c,1}$ (i.e., Type I instability). Also, they found that another mode of instability (i.e., Type II instability) for moving disturbance waves, caused by the Coriolis force, exists at much lower value of critical Reynolds number $Re_{c,2}$ compared to those of stationary disturbance waves.

Some examples of the stationary disturbances are concerned with the Type I instability described as below. The Kármán boundary-layer transition on a rotating disk was first studied by Smith (1947) using the hot-wire technique. He observed that sinusoidal disturbances appear in the disk boundary-layer at sufficiently large Reynolds numbers. Approximately 32 oscillations were observed within a disk rotation period and his numerical analysis indicated that the disturbances propagate at an angle of about 14° relative to the outward drawn radius (where the direction of disk rotation defines positive angle). Later, Gregory et al.(1955) observed 28~31 spiraling outward vortices over a rotating disk at an angle of about 14° by using the china-clay technique for flow visualization. These vortices, which appeared stationary relative to a disk, were first observed at the local Reynolds number Re=430, and transition to turbulence occurred near Re≈ 530 (see also Gregory and Walker (1960)).

The stationary disturbance wave established in a rotating disk was subsequently studied by lots of investigators. Kobayashi et al.(1980) performed a theoretical analysis in which some of the effects of Coriolis force and streamline curvature were considered. They computed the value of $Re_{c,1}$ as 261 and observed that the number of spiral vortices is 31 or 32 at $Re=297$ and that the gradient of vortex axis was decreased from 14° to 7° as Re was increased. Malik et al.(1981) numerically predicted that the critical Reynolds

number $Re_{c,1}$, for establishment of stationary disturbance wave is 287 and these vortices spiral outward at a critical azimuth angle of about $\varepsilon_{c,1}=11.2°$ (Note that the recomputed values of Malik (1986) were $Re_{c,1}=285.36$ and $\varepsilon_{c,1}=11.4°$). They observed that there are about 21 vortices at $Re=294$. Their calculated value of $Re_{c,2}$ for Type II moving disturbance wave is about 49. Faller (1991) considered the effects of Coriolis force and streamline curvature in his stability analysis and obtained the neutral stability results, e.g, critical Reynolds number $Re_{c,1}=285.3$, critical wave number $\alpha_{c,1}=0.378$ and critical azimuth angle $\varepsilon_{c,1}=13.9°$ for Type I instability, while $Re_{c,2}=69.4$, $\alpha_{c,2}=0.279$, and $\varepsilon_{c,2}=-19.0°$ for Type II instability.

The usefulness of the e^n method for predicting transition in two-dimensional and axially symmetric flows is well established. The generally accepted value of n is 9. Accordingly, the existence of a transitional flow is within $410<\mathrm{Re}<590$ by Chin and Litt's experiment (1972). The stability analysis of rotating disk flow, (i.e., the Kármán boundary-layer) in which the effects of Coriolis force and streamline curvature are included was performed by Hwang and Lee (2000). Their study shows that the flow is always stable for a disturbance whose dimensionless wave number α is greater than 0.75 (i.e., if $\omega_D=0.325$ rps, and whose corresponding physical wave number $\bar{\alpha}>4.27\ \mathrm{cm}^{-1}$). Also, they showed that the azimuth angle of disturbance wave which spiral outward tend to be decreased from 13.2° to 9° as the local Reynolds number is further increased from $Re_{c,1}$.

In this study, the spatial and temporal stability analyses and experiments have been performed. Spatial amplification contours have been computed both the stationary disturbance wave (i.e., $C_p=0.0$) at the azimuth angle of $\varepsilon=11.29°$, 12°, 13.3° and 15° and the moving disturbance wave at the azimuth angle of $\varepsilon=12.5°$, 13.3 and 15°. As a consequence of numerical results, the value of transition point is predicted as $\mathrm{Re}\approx588$ at $\varepsilon=13.3°$ corresponding to the moving disturbance amplification of e^{10}.

Also, temporal amplification contours have been computed for the stationary disturbance waves from the azimuth angle of $\varepsilon=11.29°$, 12°, 13.3° and 15° and the moving disturbance wave at $\varepsilon=12°$, 13.3° and 15°. As a consequence of results, the value of transition point is predicted as $\mathrm{Re}\approx530$ at $\varepsilon=12°$ corresponding to the disturbance amplification of e^{10}.

The point of instability value is suggested as $\mathrm{Re}\approx463$ (r=12.7 cm) at $\varepsilon=11.5°$ corresponding to the moving disturbance amplification of e^7 and as constant physical wave number A=4.5 and spatial amplification $A_S=3.5$ corresponding to the stationary disturbance amplification contours.

2. The Governing Equations and Numerical Method

2.1 Base flow equation

The steady, laminar, axi-symmetric flow of an incompressible viscous liquid, which occupies the semi-infinite region on one side of the rotating infinite disk, was first discussed by von Kármán (1921). The similarity equations for the steady laminar base flow of Kármán boundary-layer (with the rotation system in Fig. 1) are well known; see, Faller (1991). Assuming an axi-symmetrical similarity solution to the base flow with the dimensionless velocities of x, y, z components $F(z)$, $G(z)$ and $H(z)$

$$U=\Delta\omega rF,\ V=\Delta\omega rG,\ W=\Delta\omega DH \qquad (1)$$

and scaling lengths by D and time by rotational disk speed $\omega_D{}^{-1}$, the radial and tangential base flow equations are

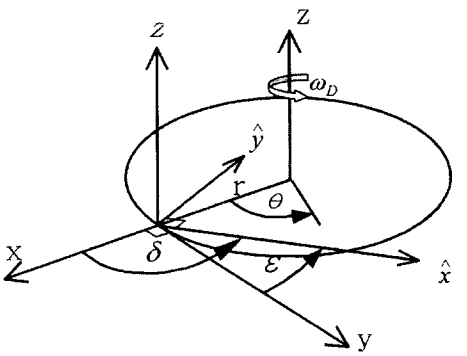

Fig. 1 Rotation system

$$F^2+HF_z-G^2+2G+F_{zz}=1 \tag{2a}$$

$$2FG+HG_z-2F-G_{zz}=0 \tag{2b}$$

The continuity equation is

$$H=-2\int_0^z F(z)\,dz \tag{3}$$

The boundary conditions are

$$F(0)=G(0)=H(0)=0,\ F(\infty)=0,\ G(\infty)=1 \tag{4}$$

The boundary-value problem (2)-(4) was solved on the interval $[0,\ \eta_\infty]$ with $\eta_\infty=40\sim240$. Namely, the base flow solution is crudely obtained first by using a finite difference method (FDM). Then, a computing code COLNEW (Bader and Ascher, 1985), which was designed to accurately solve two-point boundary-value problems, was used to find more accurate numerical solution. At that time, the crude solution was used only to provide the initial guess for COLNEW. The resulting solutions are stored as B-spline coefficients in order to be called during the stability computation.

2.2 The linear stability equations

Hwang and Lee (2000) reformulated the governing stability equation prepared by Faller (1991). From their non-dimensional perturbation equations, the rectangularized horizontal component of vorticity equations are then

$$\begin{aligned}&\xi_t+Re(F\xi_x+G\xi_y-F_zu_x-G_zu_x-G_{zz}w)\\&+Ro(H\xi_z+H_z\xi-Fv_z-F_zv-2Gu_z-G_zu+Fw_y)\\&-Cou_z=\nabla^2\xi\end{aligned} \tag{5a}$$

$$\begin{aligned}&\eta_t+Re(F\eta_x+G\eta_y-F_zv_y+G_zu_y+F_{zz}w)\\&+Ro(H_z\eta+H\eta_z+F_zu+Fu_z-2Gv)-Cov_z=\nabla^2\eta\end{aligned} \tag{5b}$$

The above equations (5a, b) is now rotated through an angle δ as illustrated in Fig. 1, where ε is the angle of the new $\hat{x}$ axis with respect to the tangential direction. The instabilities are assumed to be 2-dimensional vortices independent of new $\hat{x}$-direction, so in the rotated equations $\partial/\partial\hat{x}=0$.

The stream function for the flow in the new $(\hat{y},\ \hat{z})$-plane is defined by

$$w=\frac{\partial\phi}{\partial y},\ v=-\frac{\partial\phi}{\partial z},\ \xi=\nabla^2\phi \tag{6}$$

where $\hat{}$ will be deleted for convenience. The perturbation velocity u and stream function ϕ may be assumed as

$$\begin{aligned}u(y,\ z,\ t)&=U(z)\exp i[(\bar{\alpha}_R+i\bar{\alpha}_I)y-(\bar{\beta}_R+i\bar{\beta}_I)t]\\\phi(y,\ z,\ t)&=\Phi(z)\exp i[(\bar{\alpha}_R+i\bar{\alpha}_I)y-(\bar{\beta}_R+i\bar{\beta}_I)t]\end{aligned} \tag{7}$$

The reoriented equations with expression of Eqs. (6)-(7) are

$$\begin{aligned}&U''(z)-RoHU'(z)+i[\beta+Re(FC+GS)\alpha+i(RoF-\alpha^2)]U(z)\\&-(2RoG+Co)\Phi'(z)-Re(-F'S+G'C)i\alpha\Phi(z)=0\end{aligned} \tag{8a}$$

$$\begin{aligned}&\phi''''-RoH\,\Phi'''+i[\beta+Re(FC+GS)\alpha+i(RoH'+RoF+2\alpha^2)]\Phi''\\&-Ro[F'-H\alpha^2-C(F'C+G'S)]\Phi'\\&-[i\beta\alpha^2+Re(FC+GS)i\alpha^3+Re(F''C+G''S)i\alpha\\&+RoH'\alpha^2+Ro\alpha^2S(FS-GC)+Ro\alpha^2C(GC-FS)+\alpha^4]\Phi\\&+(2RoG+Co)U''-Ro[S(F'C+G'S)-2G']U=0\end{aligned} \tag{8b}$$

In order to specify the problem completely, boundary conditions are applied to the eigenfunctions $U(\eta)$ and $\Phi(\eta)$. Evidently, the velocity disturbances quantities u, v and w must be zero at the rotating disk surface and at a large distance out $(\eta\to\infty)$. Therefore, the non-dimensional boundary conditions are:

$$\begin{aligned}&U(0)=\Phi(0)=\Phi'(0)=0\\&U'(\infty)=\Phi(\infty)=\Phi''(\infty)=0\end{aligned} \tag{9}$$

The reformulated stability Eqs. (8a, b) with boundary conditions (9) are complex-valued, 6th-order, linear system of homogeneous differential equations.

2.3 Numerical method

The boundary conditions (9) are modified slightly but significantly. These conditions are expressed in the real and imaginary parts,

$$\begin{aligned}&U_R(0)=U_I(0)=\Phi_R(0)=\Phi_I(0)=0,\ |\Phi_R'''(0)|=|\Phi_I'''(0)|=J\\&U_R'(\infty)=U_I'(\infty)=\Phi_R(\infty)=\Phi_I(\infty)=\Phi_R''(\infty)=\Phi_I''(\infty)=0\end{aligned} \tag{10}$$

with $10^{-3}\le|J|\le10^{-1}$.

The computing procedure which use as the orthogonal collocation code COLNEW for obtaining the neutral stability curve is quite similar to

that employed in simple and multiple shooting (Hwang and Lee, 2000).

3. Results and Discussion

Classical hydrodynamic linear stability theory is based on an eigenvalue analysis of the linearized equations of motion on the characteristics of the fastest growing normal mode. A flow is deemed unstable if there exists a normal mode with a positive growth rate for the given mean conditions.

In neutral stability analysis, the basic mean flow parameter is the Reynolds number, Re. The minimum Re for which the flow is unstable is called the critical Reynolds number, Re_c. It is assumed that there are fluctuations in nature that will provide an initial perturbation at the wavelength of the most unstable mode which will then proceed to grow faster than any other normal mode and dominate the instability as long as nonlinear effects remain unimportant.

In this study, the spatial and temporal stability analyses have been performed successfully for predicting the instability. The Type I instability mode appears in the form of stationary spiral vortices at large Re and positive angles direction of ε between the tangent line and circle which was drawn radius over the disk in Fig. 1. Whereas the Type II mode instability, also, has the form of spiral vortices, but, at low Re and negative angle of ε, relatively, its vortices move rapidly outward.

We performed the stability computation at azimuth angles specified in the Table. 1. We obtained the neutral stability results for several ε values in the range $-27.3° \leq 19.1°$. (see Fig. 2, $Cp \neq 0$) In addition, we computed the spatial amplification contours at the azimuth angle $\varepsilon = 12.5°$, 13.3° and 15° and the temporal amplification contours at the azimuth angle $\varepsilon = 12°$, 13.3° and 15° near the 'nose' of the neutral stability curves.

The present stability Eqs. (8a, b) are slightly different with those of Faller (1991), but our obtained results, in particular, on Type II instability are considerably different. However, both

Table 1 Azimuth angles numerically calculated for the stationary disturbance wave & the moving disturbance wave

Amplification	Type of Waves	
	Stationary wave	Moving waves
Spatial	11.29°, 12°, 13.3°, 15°	12.5°, 13.3°, 15°
Temporal		12°, 13.3°, 15°

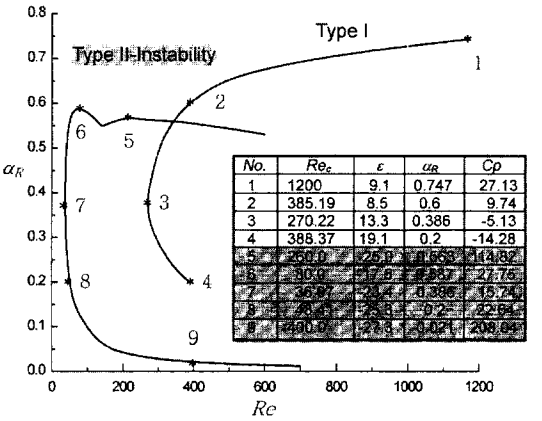

Fig. 2 4-dim. neutral stability curves for the Kármán layer

results agree within reasonable limit, considering characteristic of both neutral stability curves are almost the same.

The results show that the flow is always stable for the disturbance whose wave number $\alpha_R > 0.75$ at the neutral stability curve of the moving wave. The first unstable condition for Type II instability mode is the band of wave numbers $0.0 < \alpha_R \leq 0.587$ with azimuth angles $-27.3° \leq \varepsilon \leq -13.6°$. Also, the similar condition for Type I instability mode is $0.2 \leq \alpha_R \leq 0.75$ with $8.2° \leq \varepsilon \leq 19.1°$. These two stability results are rather more complete and they give relatively lower values of critical Reynolds numbers than those of Faller (1991).

The spatial amplification contours for the stationary disturbance waves are presented in the Re-ε plane : see Fig. 3.

Our neutral stability results are presented in terms of a parameter A, which has no r-dependence, where

$$A = \alpha_R Re^{1/2} \tag{11}$$

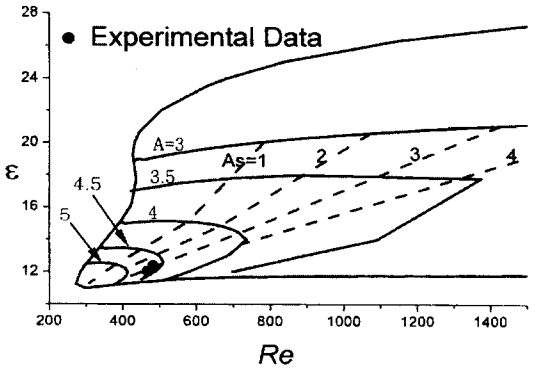

Fig. 3 Spatial amplification contours for the Kármán layer, corresponding to the Type I stationary disturbances in the Re-ε plane

The parameter A is proportional to the physical wave number $2\pi/L$ (where L is the wavelength). If $Re=457$ is fixed, the spatial amplification rate (A_S) is increased as the azimuth angle is decreased from 14° to 11° in Fig. 3. This figure shows that the physical wave number A is bounded within 3~5. Surely, this is the reason why the azimuth angle is shown in the limited angle. Also, some of our neutral stability results are presented in the Re-B plane, where

$$B=\beta_R Re^{1/2}=\frac{2\pi f D^{1/2}}{\omega_D} \tag{12}$$

This parameter B has no r-dependence: it is proportional to the physical frequency f. Constant frequency paths are horizontal straight lines in the stability Re-B plane: see Fig. 4. But, the wave number α_R corresponding to the constant value of B nonlinearly decreases as Re increases. (Namely, the wavelength gradually increases as the radius increases)

The concept of constant physical wave number or frequency is important in interpreting the physical implications of our numerical results on spatial amplification and temporal amplification, since a path of constant physical wave number or frequency corresponds to a path on the stability plane as a disturbance travels downstream in the primary period. The basic premise here is that the physical wave number of a stationary disturbance and the physical frequency of a moving disturbance will not change while the disturbance is still small even in stability plane.

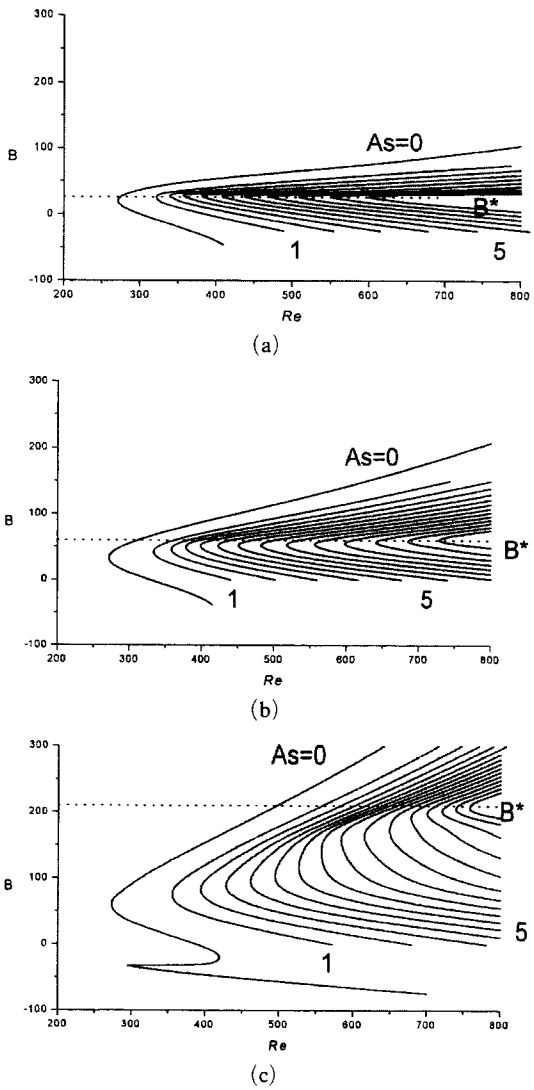

Fig. 4 Spatial amplification contours for moving disturbances at (a) $\varepsilon=12.5°$, (b) 13.3°, and (c) 15° in the Re-B plane

The spatial amplification rate of a disturbance (e^{A_S}) can be obtained for the constant frequency as follows:

$$A_S=-\int_{Re_0}^{Re}\frac{\alpha_I}{D_1}dRe=\int_{Re_0}^{Re}\alpha_I D^{-1/2}Re^{-1/2}dRe \tag{13}$$

where Re_0 is the Reynolds number on the neutral curve and D_1 is the boundary-layer thickness newly defined. The neutral curve thus corresponds to $A_S=0$. From the amplification contours

Table 2 Numerical results of constant physical frequency B* from $\varepsilon=12.5$ to 15°

Amplification	$\varepsilon(°)$		
	12.5	13.3	15
Spatial	26	60	210

Table 3 Numerical results from $\varepsilon=11.29$ to 15°

ε	Re_{crit}	β_R	α_R	B
11.29	271.43	0.0	0.390	0.0
12.0	270.86	0.8045	0.400	13.24
13.3	270.22	1.9807	0.386	32.55
15.0	271.02	3.5517	0.380	58.47

in Fig. 4, the most stimulated amplifying frequency which is well sustained primary constant physical frequency increases from B=26 to 210 as the angle of ε increases from 12.5° to 15°.

The primary starting value of constant physical frequency is calculated as shown in Table 2.

The temporal amplification rate of a disturbance (e^{A_T}) can be obtained for the constant frequency as follows;

$$A_T=\int_{t_0(Re_0)}^{t(Re)}\beta_i\frac{U}{D_1}dt=\int_{(Re_0)}^{(Re)}\beta_i D^{-1/2}Re^{-1/2}dRe \quad (14)$$

where Re_0 is the Reynolds number on the neutral curve. The neutral curve is thus $A_T=0$.

From the amplification contours in Fig. 5, the favored amplifying frequency which is well sustained primary value increases from B=10 to 75 as the angle of ε increases from 12°, 13.3° and 15°. The primary starting value of constant frequency is shown in Table 3.

From the above spatial and temporal amplification contours, at the frequency of $\varepsilon=15°$, the small disturbance is amplified quickly by as much as e^{10} as it travels downstream from $Re_0=279.80$ to $Re=544.83$. We find out that the most favored frequency decreases as ε decreases from 15° to 11.29°. In addition, the value of Re_{crit} has a minimum at $\varepsilon=13.3°$. (see, Table 3)

Although it is known that the linear stability theory can be used only for predicting of instability at the low Reynolds number, we obtained the reasonable full details of amplification contours at the larger Reynolds number for various ε's.

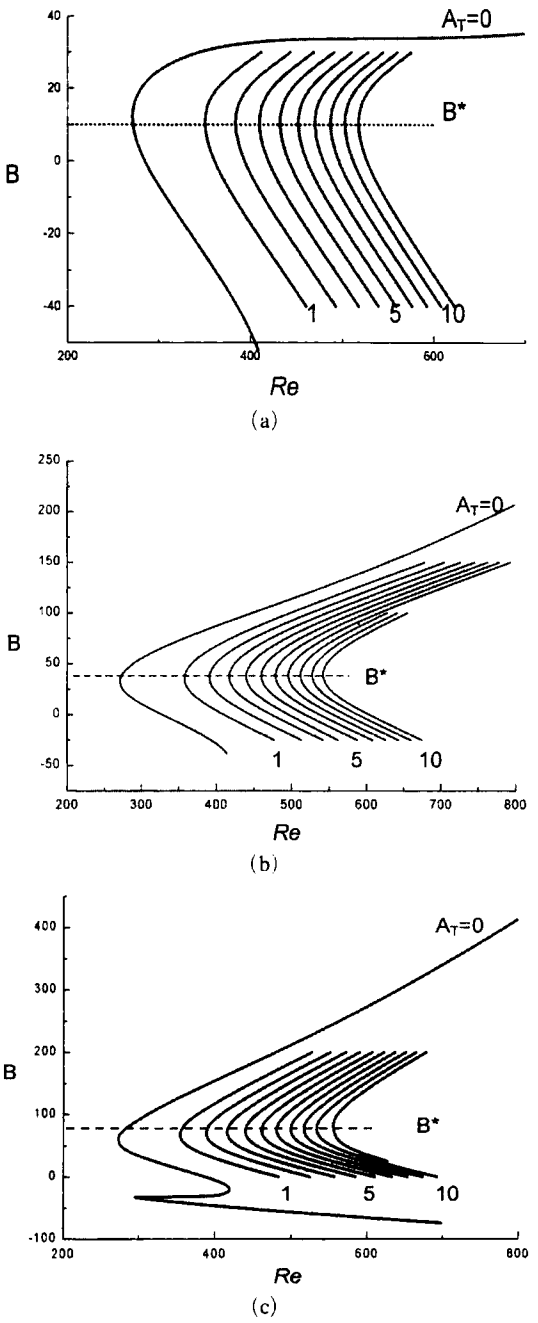

Fig. 5 Temporal amplification contours for (a) $\varepsilon=12°$ (b) $\varepsilon=13.3°$ and (c) $\varepsilon=15°$ in the (Re, B)-planes

Table 4 Experimental results from 1200 rpm to 1800 rpm

Revolution per Minute	1200	1400	1600	1800
Distance from center to the point of instability	164.9	155.8	140.3	127.1
Distance from center to the point of transition to turbulent (mm)	183.9	172.6	165.9	150.7
Re at the point of instability	490.2	500.4	481.8	462.8
Re at the point of transition to turbulence	546.7	554.3	569.6	548.7

Table 5 Reynolds number at the point of instability

Description	Re at the point of instability
Experimental Results	462~500
Gregory et al.(1955)	430
Chin and Litt (1972)	410~510

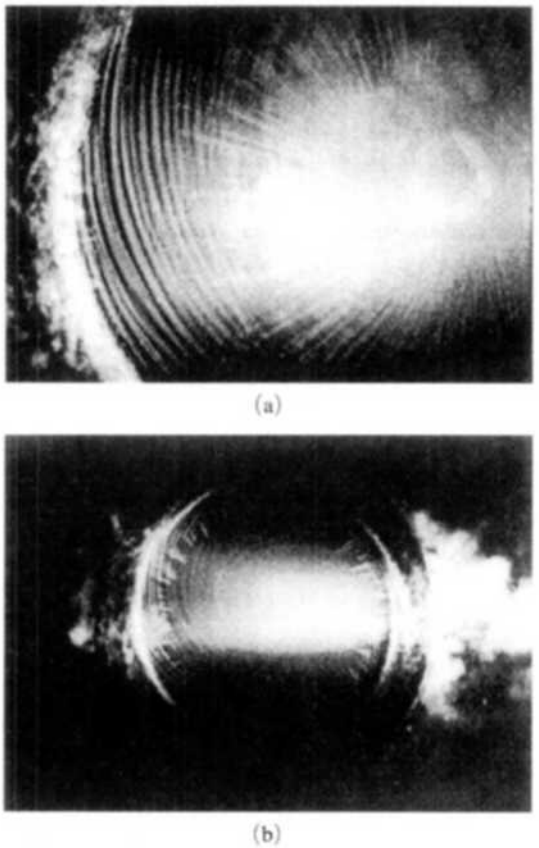

Fig. 6 Flow pattern on a disk rotating in air at (a) 1600 and (b) 1800 rpm by using a white titanium tetrachloride gas

The hydrodynamic instability of Kármán boundary-layer flow due to a rotating disk has been experimentally investigated for the disturbance waves. The disturbed flow was observed using a smoke visualization apparatus over rotating disk system. In the stationary disturbance waves, about 30 spiral vortices are observed. The faster the disk rotates from 1200 rpm to 1800 rpm, the shorter the distance from the center of the disk to the point of instability and the point of transition is. (see, Table 4 and Fig. 6) When we compared the stability results and experimental data of the present work with the experimental data of Gregory et al.(1955) and Chin and Litt (1972) for the stationary disturbance wave, the numerical and experimental results agree comparably with the previous experimental data. (see, Fig. 3 and Table 5)

4. Conclusions

The stability of the 3-D boundary-layer flow introduced in a rotating disk system has been numerically studied by employing the linear stability theory and experimented. The modified stability equations are accurately solved by eigenfunction analysis as a two-point boundary-value problem. The results yield more complete 4-dimensional neutral stability curves corresponding to the Type I and II instabilities.

Spatial and temporal amplification contours have been computed for both the moving disturbance wave and stationary disturbance wave. From the spatial amplification contours for moving disturbances in Fig. 4, the wave number α_R corresponding to the constant value of B nonlinearly decreases as Re increases. The most stimulated amplifying frequency which is well sustained primary constant physical frequency increases from B=26 to 210 as the angle of ε increases from 12.5° to 15°. From the temporal amplification contours for moving disturbances in Fig. 5, the